Energy Conversion and Management 220 (2020) 113100

Contents lists available at ScienceDirect

Energy Conversion and Management

journal homepage: www.elsevier.com/locate/enconman

The equivalent low-dissipation combined cycle system and optimal analyses of a class of thermally driven heat pumps

Juncheng Guo[a,b,*], Hanxin Yang[a], Julian Gonzalez-Ayala[b,c], J.M.M. Roco[b,c], A. Medina[b,c], A. Calvo Hernández[b,c]

[a] College of Physics and Information Engineering, Fuzhou University, Fuzhou 350116, People's Republic of China
[b] Department of Applied Physics, University of Salamanca, 37008 Salamanca, Spain
[c] Instituto Universitario de Física Fundamental y Matemáticas (IUFFyM), University of Salamanca, 37008 Salamanca, Spain

ARTICLE INFO

Keywords:
Thermally driven heat pump
Three-heat-source cycle model
Low-dissipation assumption
Performance bound
Optimal analyses

ABSTRACT

The performance characteristics, operation, and design strategies of a class of thermally driven heat pumps are investigated due to their important roles in the efficient utilization of low-grade thermal energy. In order to establish a more generic thermodynamic model of thermally driven heat pumps mainly including absorption, adsorption, and ejector heat pumps, low-dissipation assumption is adopted. Accordingly, the associated dissipation parameters accounting for the specific information on the irreversibilities in each heat-transfer process are introduced rather than specifying heat-transfer law. Based on the proposed model, the theoretical results of the coefficient of performance and heat load are derived with regard to two key parameters denoting the size ratio of the two involved subsystems and the matching deviation from reversible limit. The performance characteristics and the optimally operating regions of the whole system are determined and the differences between thermally driven heat pump and refrigerator are highlighted. The proposed model and obtained results further develop the low-dissipation model and may provide a useful description for the operation and design of practical thermally driven heat pumps.

1. Introduction

In recent decades, motivated by the ever-increasing energy requirement and the continuously growing challenges about environmental pollution and climate change related to the intensive usage of fossil fuel, the effective utilization of low-grade thermal energies, such as solar energy, industrial waste heat, geothermal energy, and so on, has attracted much attention from both engineers and researchers [1]. Various feasible low-grade heat harvesting technologies, such as organic Rankine cycle [2], thermoelectric devices [3], and electrochemical system [4], have emerged successively. Among all, a class of thermally driven heat pumps, mainly including absorption [5], adsorption [6], and ejector [7] heat pumps, are nowadays some of the most competitive and promising due to their low capital cost, low noise, high reliabilities, and wide adaptability to various low-grade heat sources with different temperatures and become a hot research topic. The influences of working pairs on the performance of absorption [8] and adsorption [6] heat pumps are investigated. The nozzle configuration [9], phase transitions [10] are taken into account in the performance evaluations of ejector heat pumps. The practical applications of thermally driven heat pumps e.g., heating [11], drying [12], desalination [13], and cogeneration [14] are proposed and discussed respectively. In addition, various hybrid system such as compression-absorption heat pump [15] ejector-compressor heat pump [16], fuel cell-based hybrid system [17], combined cooling, heating and power system [18], and solar-driven heat pump [19] are put forward.

On the other hand, despite the differences of working fluids, components, and circulation modes involved in various types of thermally driven heat pumps, they have the basic operating principle in common from the viewpoint of thermodynamics. Consequently, many researchers try to explore the performance bounds of thermally driven heat pumps by presenting theoretical models. On the basis of classical thermodynamics, the performance of this class of heat pumps may be described by a reversible three-heat-source cycle [20] which is equivalent to a combined cycle system consisting of a reversible Carnot heat pump driven by a reversible Carnot heat engine. The coefficient of performance (COP) of the heat pump is given by [20]

$$\psi_r = \frac{T_P}{T_H}\frac{T_H - T_O}{T_P - T_O} \tag{1}$$

* Corresponding author at: No.2 Wulongjiangbei Road, Fuzhou, China.
E-mail address: junchengguo@qq.com (J. Guo).

https://doi.org/10.1016/j.enconman.2020.113100
Received 29 February 2020; Received in revised form 8 June 2020; Accepted 9 June 2020

Nomenclature

Latin letters

C	size ratio of two subsystems
N	mass (mol)
Q	heat (J)
R	heat load (W)
$\tilde{R}$	dimensionless heat load
S	entropy (JK^{-1})
T	temperature (K)
$\tilde{T}$	dimensionless temperature
t	time (s)
$\tilde{t}$	dimensionless time
U	energy (J)
W	work (J)

Greek letters

α	parameter of deviation from reversible limit
β	dissipation symmetry between two subsystems
γ	temporal symmetry between two subsystems
ε	coefficient of performance of Carnot heat pump
η	efficiency of Carnot heat engine
μ	chemical potential ($Jmol^{-1}$)
σ	dissipation parameter (s)
$\tilde{\sigma}$	dimensionless dissipation parameter
τ	cycle time (s)
$\tilde{\tau}$	dimensionless cycle time
ψ	coefficient of performance of the three-heat-source heat pump

Subscript

ce	chemical engine
cp	chemical pump
H	high temperature side/source
P	heated space
PH	heated space side in Carnot heat engine
PO	heated space side in Carnot heat pump
he	heat engine
hp	heat pump
max	maximum
min	minimum
O	low temperature side/source
Rm	maximum heat load state
r	reversible condition

Abbreviations

COP	coefficient of performance

where T_O, T_P, and T_H are respectively the temperatures of environment, heated space, and the low-grade heat reservoir. The reversible value ψ_r determining the COP bound of the thermally driven heat pump for given operating temperatures has greatly theoretical significance but its practical value is limited since the heat load of the thermally driven heat pump is equal to zero when the COP achieves ψ_r.

In order to explore the performance of a practical thermally driven heat pump with finite heat load, an endoreversible three-heat-source thermodynamic cycle model has been adopted [21], in which the irreversibilities associated to the coupling of the working fluid to external heat baths have been discussed and evaluated. Many authors have further considered the influences of internal irreversibilities of the working fluid [22], external heat leakage losses [23], different heat-transfer laws [24], and the temperature difference between absorber and condenser [25]. Besides, in order to provide more comprehensive optimization criteria, different objective functions, e.g., thermo-economic function [26] and ecological function [27], have been introduced. Moreover the performance characteristics of related hybrid systems such as fuel cell-based hybrid system [28], geothermal heat-engine-driven heat pump [29], and solar-driven heat pump [30] have been discussed.

However, it is well known that the performance characteristics of endoreversible and irreversible Carnot-like cycles are dependent on the heat-transfer laws between the external heat reservoirs and the working fluid closely [31]. In other words, different laws of heat-transfer lead to different performances [32]. Due to this limitation, the search of more universal thermodynamic cycle is a highly desirable and necessary task. In 2010, a low-dissipation thermodynamic cycle model was proposed by Esposito et al. [33] without adopting a specific law in the heat-transfer processes. Two important and valuable features of the low-dissipation model are the explicit role played by the time durations of the heat transfers and the irreversibilities parameters in each of such processes, allowing the explicit analysis of possible symmetries/asymmetries in the model. With the help of low-dissipation assumptions, the upper and lower bounds of the maximum power efficiency of Carnot heat engine were obtained. More importantly, several famous results derived from endoreversible thermodynamic cycle model under different heat-transfer laws can be directly recovered by using the low-dissipation model [33].

Low-dissipation models provided a new approach to study the performance of thermodynamic devices and gained the interest of numerous researchers. It has been applied to establish and analyze the performance characteristics of various thermodynamic devices such as Carnot refrigerator [34], Carnot-like heat engines [35], generalized Carnot chemical engines [36], generalized quantum thermal devices [37], and so on. In addition, the performance characteristics of χ function [38] and Ω function [39] and under time constraint [40], size constraint [41], and universal constraint [42] for both heat engines and refrigerators have been investigated. Furthermore, the relations between low-dissipation, minimally nonlinear irreversible thermodynamic cycles [43], and endoreversible [44] models have been discussed. It is worthy to emphasize that this generality and universality of low-dissipation model originates from the nature of many irreversible energy converters. Specifically, the first order time-related entropy generation of these thermodynamic devices behave as $1/t$ [45].

However, for a long time after the proposition of low-dissipation model, its application has been confined mainly to thermal devices coupled to only two heat sources in spite of its proved wide generality. In Ref. [46], low-dissipation model has been firstly adopted to construct a combined cycle model of thermally driven refrigerators coupled to three heat sources simultaneously. As a counterpart of thermally driven refrigerator, thermally driven heat pumps have similar operating principle but well different technological applications, different operating temperatures, and different objective functions. However, literature survey shows that they have not been discussed within the framework of low-dissipation model. Consequently, it is of great significance both in theory and in practice to further establish a more generic thermodynamic model of the thermally driven heat pump by using low-dissipation assumptions and discuss the performance characteristics under the influences of heat-transfer time durations, symmetry/asymmetries conditions induced by irreversibilities, and the coupling constraints imposed by the entropy generation of the whole system. In addition, it is of interest to explore the different performance characteristics and design constraints between the low-dissipation

models of thermally driven refrigerators and heat pumps. This is the main objective of the paper, which is structured as follows.

In Section 2, an absorption heat pump is described along with a universally equivalent low-dissipation thermodynamic model. Accordingly, the expressions of COP and heat load of the model are derived and the optimal relation between them are discussed. Section 3 contains the main energetic results of this paper: the performance and the optimal operation regions of the model are investigated and revealed. The influence of the temporal and dissipative symmetries and other coefficients on the performance of the model are numerically evaluated. The bounds of the COP at maximum heat load are obtained. The different performance characteristics and design constraints between thermally driven refrigerators and heat pumps are specially stressed. A further extension and a limit case of the proposed model are discussed, which highlights its validity and generality. Besides, the limitations of the proposed model are presented. Finally, the concluding remarks are presented in Section 4.

2. Model description and the optimal relation between performance functions

In this section, the descriptions of a thermally driven heat pump and its equivalent low-dissipation combined cycle model are given by which the analytical expressions of COP and heat load are derived and the optimal relation between them is discussed.

2.1. Thermally driven heat pump and its equivalent low-dissipation combined cycle model

Fig. 1 shows the schematic diagram of an absorption heat pump operating between three heat reservoirs with temperatures T_O, T_P, and T_H, corresponding to environment, heated space, and high-temperature heat source, respectively. Comparing to traditional compression heat pump, the condenser and evaporator have no difference, but the compressor has been replaced by generator and absorber. More importantly, low-grade thermal energy is used to drive this system instead of consuming electricity. To be more specific, in the generator heat is absorbed by the refrigerant-absorbent mixture from high-temperature reservoir in order to separate the refrigerant. And then the refrigerant is transported along the condenser, throttle valve, and evaporator. After that the refrigerant transported from evaporator is absorbed by the absorbent in the absorber and releases heat into the heated space. As a result, after going through the absorber and generator, gaseous refrigerant with low temperature and pressure is translated into gaseous refrigerant with high temperature and pressure. In other words, the function of compressor in a traditional heat pump is fulfilled here by the joint works of generator and absorber: the difference between the heats exchanged with high-temperature reservoir and heated space can be regarded as the work generated by a heat engine driving the compressor.

In Fig. 1, Q_H, Q_{PH}, Q_{PO}, and Q_O denote, respectively, the heat absorbed by the generator from the high-temperature heat reservoir, the heats released into the heated space by the absorber and condenser, and the heat absorbed by the evaporator from environment. All these magnitudes are expressed in regard to one cycle time. The working fluid is recirculated by a circulation pump driven by a small amount of electrical energy, which is usually assumed to be negligible [47].

It should be mentioned that absorption, adsorption, and ejector heat pumps have the fundamental principle in common from the viewpoint of thermodynamics in spite of their different constructions, working substances, and circulation modes. Therefore, instead of study the specific models of adsorption and ejector heat pumps, a generic and unified model which may be used for the description of a class of thermally driven heat pumps will be proposed in the following.

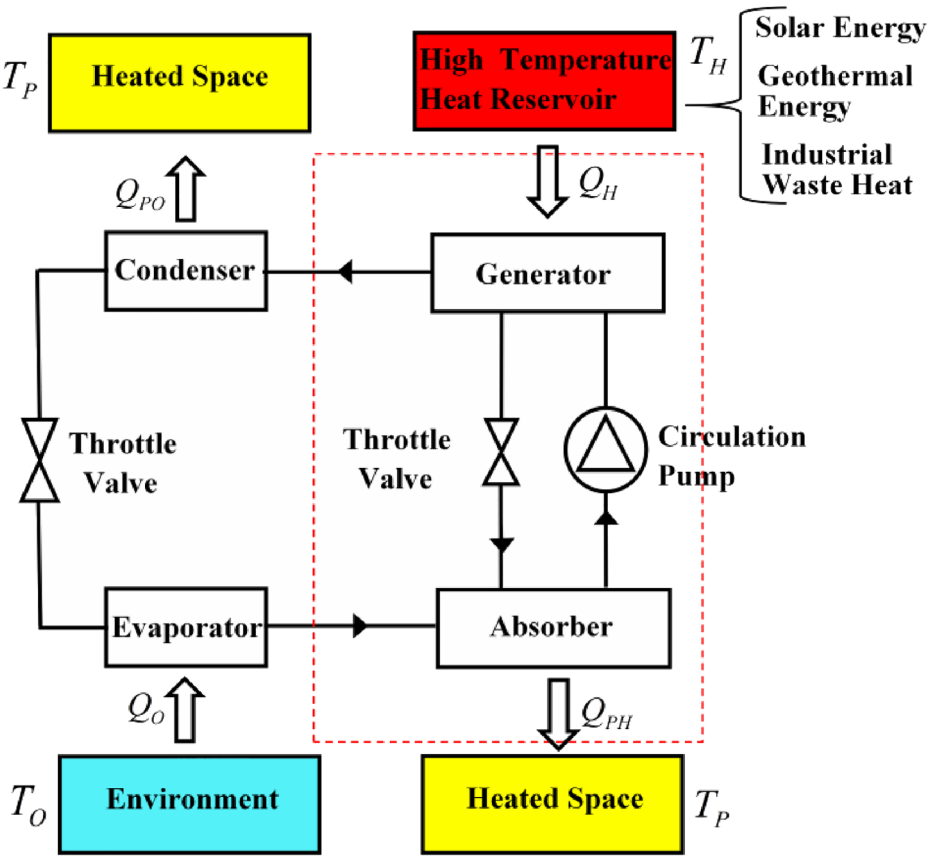

Fig. 1. The schematic diagram of the absorption heat pump.

According to low-dissipation assumptions [33], an equivalent low-dissipation combined cycle model of thermally driven heat pumps consisting of a low-dissipation Carnot heat pump driven by a low-dissipation Carnot heat engine is established, as shown in Fig. 2. In this model the time durations of heat-exchanging processes and the associated dissipation parameters in all heat-exchanging processes are well defined. Specifically, t_H, t_{PH}, t_{PO}, and t_O denote, respectively, the time durations of four heat-exchanging processes inside cycle. To be more practical, t_H, t_{PH}, t_{PO}, and t_O indicate the heat-exchanging time durations inside generator, absorber, condenser, and evaporator for the absorption heat pump; the heat-exchanging time durations inside desorber, adsorber, condenser, and evaporator for the adsorption heat pump; the heat-exchanging time durations inside generator, condenser ($t_{PH}+t_{PO}$), and evaporator for the ejector heat pump. σ_H, σ_{PH}, σ_{PO}, and σ_O are the four corresponding non-negative dissipation parameters with the specific information on the irreversibilities. It is worth of noting that the physical meanings of the dissipation coefficients are somewhat abstract and hard to be determined for realistic thermal devices. Nevertheless, low-dissipation model still draws great attention of researchers due to its generality, wide applicablity, and inherent links with other theoretical models. Researchers mainly focused their attention on the significant and universal results derived from dissipative and temporal symmetries/asymmetries analyses.

2.2. Coefficient of performance and heat load

Based on low-dissipation assumptions, the times spent in the adiabatic processes and the relaxation time of the working fluid can be ignored compared to the time durations of heat-exchanging processes in the cycle. Besides, the energy dissipations of heat reservoirs along heat-exchanging processes of Carnot heat engine and Carnot heat pump are assumed to expressed as σ_H/t_H, σ_{PH}/t_{PH}, σ_{PO}/t_{PO}, and σ_O/t_O, respectively, by neglecting the terms with more complicated time-dependence. Consequently, Q_H, Q_{PH}, Q_{PO}, and Q_O can be expressed, respectively, as [33]

$$Q_H = Q_{Hr}\left(1-\frac{\sigma_H}{t_H}\right) = T_H\Delta S_{he}\left(1-\frac{\sigma_H}{t_H}\right) \tag{2}$$

$$Q_{PH} = Q_{PHr}\left(1+\frac{\sigma_{PH}}{t_{PH}}\right) = T_P\Delta S_{he}\left(1+\frac{\sigma_{PH}}{t_{PH}}\right) \tag{3}$$

$$Q_{PO} = Q_{POr}\left(1+\frac{\sigma_{PO}}{t_{PO}}\right) = T_P\Delta S_{hp}\left(1+\frac{\sigma_{PO}}{t_{PO}}\right) \tag{4}$$

and

$$Q_O = Q_{Or}\left(1-\frac{\sigma_O}{t_O}\right) = T_O\Delta S_{hp}\left(1-\frac{\sigma_O}{t_O}\right) \tag{5}$$

where $Q_{Hr} = T_H\Delta S_{he}$ and $Q_{PHr} = T_P\Delta S_{he}$ are, respectively, the absorbed heat from the heat reservoir with high temperature and the heat released into the heated space by the Carnot heat engine under reversible limit; $Q_{POr} = T_P\Delta S_{hp}$ and $Q_{Or} = T_O\Delta S_{hp}$ are, respectively, the heats pumped into the heated space and absorbed from the environment by the Carnot heat pump under reversible limit. ΔS_{he} and ΔS_{hp} denote, respectively, the entropy changes of Carnot heat engine and heat pump under reversible limit, and can be considered as the size scales of the corresponding thermal devices [41].

It should be pointed out that the value of the reversible entropy change in the low-dissipation models operating between only two heat reservoirs is somewhat trivial and usually adopted as one of the parameters making the performance functions, e.g., power, cooling rate, or heat load, dimensionless. Consequently, it affects merely the performance characteristics quantitatively [40]. However, it is not only important but also necessary to consider the relation between ΔS_{he} and ΔS_{hp} in regard to the low-dissipation three-heat-source heat pump due to the significant influence of the matching between the heat pump and heat engine. Using Eqs. (2)–(5) and considering the first law of thermodynamics, namely, $Q_H + Q_O = Q_{HP} + Q_{OP}$, and the fact that the size ratio of the Carnot heat pump to the Carnot heat engine must be fixed for a practical three-heat-source heat pump, one can obtain the relation between ΔS_{he} and ΔS_{hp},

$$\frac{\Delta S_{hp}}{\Delta S_{he}} = \frac{T_H\left(1-\frac{\sigma_H}{t_H}\right) - T_P\left(1+\frac{\sigma_{PH}}{t_{PH}}\right)}{T_P\left(1+\frac{\sigma_{PO}}{t_{PO}}\right) - T_O\left(1-\frac{\sigma_O}{t_O}\right)} = C \tag{6}$$

where C is a constant denoting the size ratio of the Carnot heat pump to the Carnot heat engine. According to the above analyses together with the specific description of the absorption heat pump in Section 2.1, the correspondingly practical meaning of C for the absorption heat pump can be deduced. That is, the size ratio C may correspond to the ratio of the heat exchange area of condenser (evaporator) to that of generator (absorber) for the absorption heat pump. Similarly, the size ratio C may correspond to the ratio of the heat exchange area of condenser (evaporator) to that of adsorber (desorber) for the adsorption heat pump and correspond to the ratio of the heat exchange area of evaporator to that of generator for the ejector heat pump.

It can be found out from Eqs. (2) to (5) that the low-dissipation three-heat-source heat pump will become reversible when $t_H \to \infty$, $t_{PH} \to \infty$, $t_{PO} \to \infty$, and $t_O \to \infty$. In addition, according to the physical meaning of C and Eq. (6), the value of C for a practical three-heat-source heat pump should locate in the region of

$$0 < C < C_r \tag{7}$$

where $C_r = (T_H - T_P)/(T_P - T_O)$ is the value of C at reversible condition. Based on Eq. (7), a parameter $\alpha = C/C_r$ $(0 < \alpha < 1)$ can be defined, which measures the matching deviation of the low-dissipation three-heat-source heat pump from the reversible matching limit ($\alpha = 1$). It should be pointed out that C and α are correlated for given values of the temperature of external heat reservoirs. In the following discussions, in the most cases, α is adopted because it can explicitly show the departure of C from reversible conditions, namely, C_r.

Using Eqs. (2)-(6), the heat load and COP of the low-dissipation three-heat-source heat pump can be derived, respectively, as

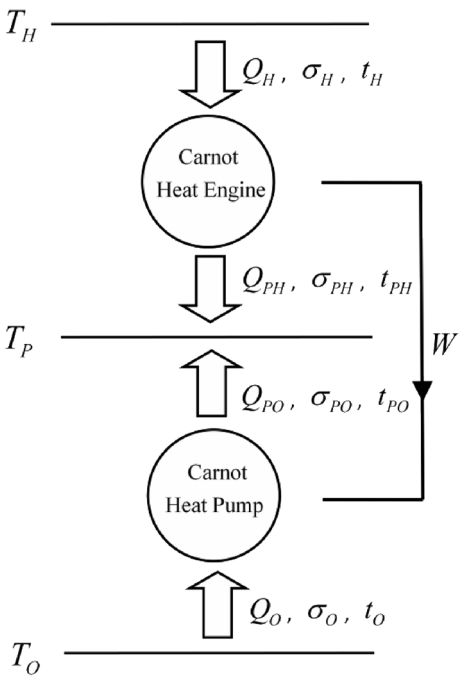

Fig. 2. The equivalent low-dissipation cycle model of a class of thermally driven heat pumps.

$$R = \frac{Q_P}{\tau} = \frac{T_H \Delta S_{he}(1 - \frac{\sigma_H}{t_H}) + T_O \Delta S_{hp}(1 - \frac{\sigma_O}{t_O})}{t_H + t_{PH} + t_{PO} + t_O} \tag{8}$$

and

$$\psi = \frac{Q_P}{Q_H} = 1 + \eta(\varepsilon - 1) = 1 + C\frac{T_O(1 - \frac{\sigma_O}{t_O})}{T_H(1 - \frac{\sigma_H}{t_H})} \tag{9}$$

where $\tau = t_H + t_{PH} + t_{PO} + t_O$ is the overall time duration of the low-dissipation three-heat-source heat pump for one cycle, $\eta = W/Q_H$ is the Carnot heat engine efficiency, and $\varepsilon = Q_{PO}/W$ is the COP of the Carnot heat pump, $W = Q_H - Q_{PH} = Q_{PO} - Q_O$ is the output work of the Carnot heat engine as well as the input work of the Carnot heat pump during one cycle.

2.3. Optimal relation between the heat load and the coefficient of performance

It can be realized from Eq. (9) that when both η and ε are optimum, the COP of a low-dissipation three-heat-source heat pump is optimum under the relevant conditions. According to the low-dissipation model established above, the low-dissipation Carnot heat engine efficiency can be derived as

$$\eta = 1 - \frac{Q_{PH}}{Q_H} = 1 - \frac{\tilde{T}_P(1 + \frac{1 - \tilde{\sigma}_H}{\tilde{\tau}_{he} - \tilde{t}_H})}{\tilde{T}_H(1 - \frac{\tilde{\sigma}_H}{\tilde{t}_H})} \tag{10}$$

where $\tilde{T}_H = T_H/T_O$, $\tilde{T}_P = T_P/T_O$, $\tilde{\sigma}_H = \sigma_H/(\sigma_H + \sigma_{PH})$, $\tilde{t}_H = t_H/(\sigma_H + \sigma_{PH})$, $\tilde{\tau}_{he} = (t_H + t_{PH})/(\sigma_H + \sigma_{PH})$. Using Eq. (10), one can prove that the relation

$$\tilde{t}_H = \begin{cases} \frac{\tilde{\sigma}_H\tilde{\tau}_{he} - \sqrt{\tilde{\sigma}_H\tilde{\tau}_{he}[\tilde{\tau}_{he} - (2\tilde{\sigma}_H - 1)](1 - \tilde{\sigma}_H)}}{2\tilde{\sigma}_H - 1}, & \tilde{\sigma}_H \neq 0.5 \\ \frac{1 + 2\tilde{\tau}_{he}}{4}, & \tilde{\sigma}_H = 0.5 \end{cases} \tag{11}$$

should be satisfied to make η optimized.

Similarly, based on the low-dissipation model established above, the COP of the low-dissipation Carnot heat pump can be given by

$$\varepsilon = \frac{Q_{PO}}{Q_{PO} - Q_O} = \frac{\tilde{T}_P(1 + \frac{1 - \tilde{\sigma}_O}{\tilde{\tau}_{hp} - \tilde{t}_O})}{\tilde{T}_P(1 + \frac{1 - \tilde{\sigma}_O}{\tilde{\tau}_{hp} - \tilde{t}_O}) - (1 - \frac{\tilde{\sigma}_O}{\tilde{t}_O})} \tag{12}$$

where $\tilde{\sigma}_O = \sigma_O/(\sigma_O + \sigma_{PO})$, $\tilde{t}_O = t_O/(\sigma_O + \sigma_{PO})$, $\tilde{\tau}_{hp} = (t_O + t_{PO})/(\sigma_O + \sigma_{PO})$. It can be proved from Eq. (12) that when ε is optimal the relation between $\tilde{t}_O$ and $\tilde{\tau}_{hp}$ is given by

$$\tilde{t}_O = \begin{cases} \frac{\tilde{\sigma}_O\tilde{\tau}_{hp} - \sqrt{\tilde{\sigma}_O\tilde{\tau}_{hp}[\tilde{\tau}_{hp} - (2\tilde{\sigma}_O - 1)](1 - \tilde{\sigma}_O)}}{2\tilde{\sigma}_O - 1}, & \tilde{\sigma}_O \neq 0.5 \\ \frac{1 + 2\tilde{\tau}_{hp}}{4}, & \tilde{\sigma}_O = 0.5 \end{cases} \tag{13}$$

Above analyses show that the COP and heat load of the proposed model depend on the following set of parameters: the dimensionless irreversibility parameters $\tilde{\sigma}_H$ and $\tilde{\sigma}_O$; the dimensionless temperatures $\tilde{T}_H$ and $\tilde{T}_P$; the dimensionless times of the heat engine $\tilde{\tau}_{he}$ and heat pump $\tilde{\tau}_{hp}$; and the parameters α and C denoting the matching deviation from the reversible limit of the global model and the size ratio of the Carnot heat pump to the Carnot heat engine, respectively. Besides, as a theoretical research about the generic and unified thermodynamic model of three-heat-source heat pump, the influence of size symmetry/asymmetry of the overall system and the dissipation symmetry/asymmetry of the subsystems and overall system on the performance characteristics are more concerned. Therefore, for the convenience of calculation and discussion, it is useful to introduce a dimensionless heat load defined by

$$\tilde{R} = \frac{R(\sigma_O + \sigma_{PO})}{T_O \Delta S_{hp}} = \frac{\frac{\tilde{T}_H}{C}(1 - \frac{\tilde{\sigma}_H}{\tilde{t}_H}) + (1 - \frac{\tilde{\sigma}_O}{\tilde{t}_O})}{\tilde{\tau}_{he}\frac{\beta}{1 - \beta} + \tilde{\tau}_{hp}} \tag{14}$$

where $\beta = (\sigma_H + \sigma_{PH})/(\sigma_H + \sigma_{PH} + \sigma_O + \sigma_{PO})$ gives a measure of the symmetry of the irreversibility (dissipation) coefficients between the involved heat engine and heat pump. In addition, an important control parameter $\gamma = \tilde{\tau}_{he}/(\tilde{\tau}_{he} + \tilde{\tau}_{hp})$ representing the ratio of the cycle time of Carnot heat engine to the whole cycle time is introduced as well. It could be considered as a measurement of the temporal symmetry of the overall system. In the next section, the influence of these parameters on the performance properties of the low-dissipation three-heat-source heat pump model will be discussed in detail.

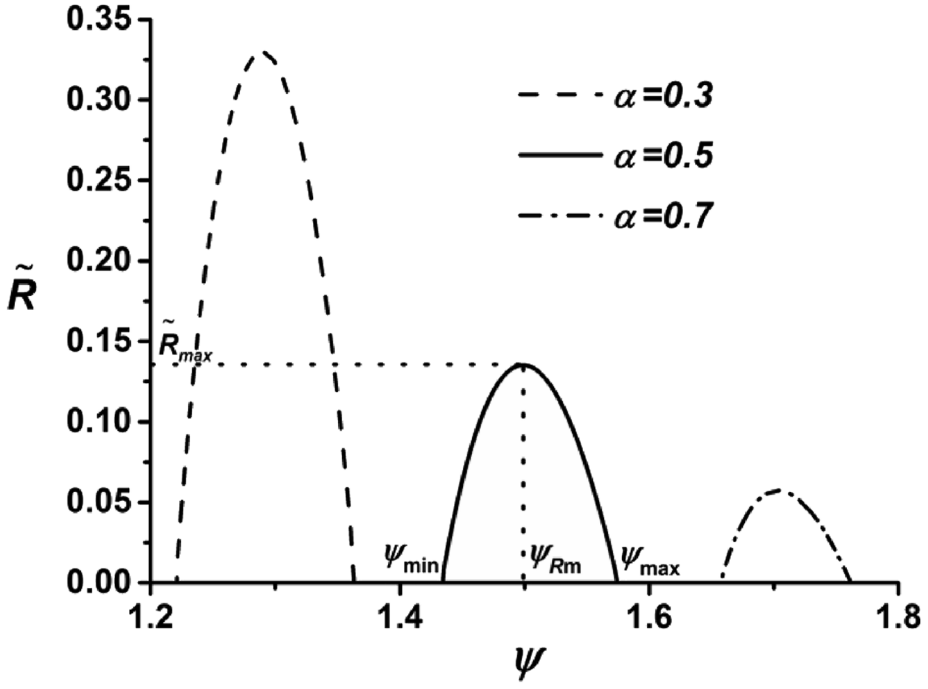

Fig. 3. The relation between optimized ψ and the corresponding $\tilde{R}$ for different values of α. Fixed parameters are $\tilde{\sigma}_H = \tilde{\sigma}_O = 0.3$, $\beta = 0.5$, $\tilde{T}_H = 3$ and $\tilde{T}_P = 1.5$.

3. Results and discussion

Based on the analyses above, the performance characteristics and the optimal operation and design strategies of the system are investigated and discussed by using numerical calculation in this section. Specially, the COP bounds at maximum heat load are obtained at extreme asymmetry conditions and the different performance characteristics and design constraints between thermally driven refrigerators and heat pumps are stressed. Moreover, a further extension and a limit case of the proposed model are presented, which highlights its validity and generality. Besides, the limitations of the proposed model are discussed.

3.1. The behaviors of optimized coefficient of performance with heat load

By using Eqs. (6), (8), (9), (11), and (13), the relation between the optimized COP and the corresponding heat load of the low-dissipation three-heat-source heat pump for different values of α can be obtained. Unfortunately, the relation deduced from Eq. (6) are not handy analytical and thus it should be investigated numerically to get explicit results.

The parametric plot of the optimized COP and corresponding heat load for the different values of α is shown in Fig. 3. It is seen from Fig. 3 that the optimal relation between $\tilde{R}$ and ψ is not monotonic and the $\tilde{R}-\psi$ curves are parabolic for a given value of α. For different selections of α, the qualitative behavior, namely, parabolic, is kept. There exist a minimum COP $\psi_{\min}$ and a maximum COP $\psi_{\max}$ at which $\tilde{R}=0$. Both $\psi_{\max}$ and $\psi_{\min}$ increase with the increase of α. Besides, an optimal value ψ_{Rm} exists making $\tilde{R}$ to achieve its maximum $\tilde{R}_{\max}$ for a given value of α. ψ_{Rm} increases with the increase of α, whereas $\tilde{R}_{\max}$ decreases with the increase of α. In addition, it can be seen from Fig. 3 that for a given value of α, when $\tilde{R}<\tilde{R}_{\max}$ there are two corresponding ψ for a given $\tilde{R}$. Specifically, one is greater than ψ_{Rm} and the other is less than ψ_{Rm}. As a consequence, the optimally operating region should be located in the region of $\psi>\psi_{Rm}$. The corresponding optimal regions of $\tilde{\tau}_{he}$ and $\tilde{\tau}_{hp}$ for given α can be determined by numerical calculation accordingly. Moreover, the associated optimal ranges of $\tilde{t}_H$ and $\tilde{t}_O$ can be further derived by using Eqs. (11) and (13). According to literature review, such a behavior between $\tilde{R}$ and ψ for the thermally driven heat pump has never been obtained previously. For a realistic thermally driven heat pump, the time durations of heat exchange processes in each components should be controlled according to the above results to make it work in the optimal region.

Similarly, the optimal curves of $\tilde{R}-\psi$ for different β and different dissipation coefficients can be generated by using Eqs. (6), (8), (9), (11), (13), and numerical calculation, as shown in Figs. 4 and 5, respectively. It can be found form Fig. 4 that the values of $\psi_{\max}$ and $\psi_{\min}$ are independent of β under given other parameters. Besides, $\tilde{R}$ and $\tilde{R}_{\max}$ decrease with the increase of β under given other parameters, which is in conformity with Eq. (14). Moreover, ψ_{Rm} increases with the increase of β for the given other parameters. Fig. 5 indicates that the value of $\psi_{\max}$ is dependent of $\tilde{\sigma}_H$ while the value of $\psi_{\min}$ depends on $\tilde{\sigma}_O$. More specifically, $\psi_{\max}$ increases with the increase of $\tilde{\sigma}_H$, whereas $\psi_{\min}$ increases with the decrease of $\tilde{\sigma}_O$. The dependences of $\tilde{R}_{\max}$ and ψ_{Rm} on $\tilde{\sigma}_H$ and $\tilde{\sigma}_O$ will be discussed detailly in Section 3.3.

3.2. The influence of γ

Likewise, the variations of the optimized COP and the corresponding heat load with γ for different values of α can be generated by similar approaches, as shown in Fig. 6.

Fig. 6 shows that the COP ψ decreases monotonically with the increase of γ but $\tilde{R}$ is not a monotonic function of γ. When $\gamma=0$ or $\gamma=1$, namely, the overall cycle time is assigned to the Carnot heat pump or the Carnot heat engine, the low-dissipation three-heat-source heat pump is disabled, i.e., $\tilde{R}=0$, which is an expected result. In addition, there exists an optimal γ_{Rm} at which $\tilde{R}$ attains its maximum $\tilde{R}_{\max}$. It can be seen from Fig. 6 that the value of γ_{Rm} increases with the decrease of α. According to the analyses in the last subsection, the optimally operating region of γ should be located in the interval $\gamma_{Rm}<\gamma<1$. In other words, the time durations of heat exchange processes in each components should be controlled to make the practical thermally driven heat pump work in the optimal region.

The dependence of γ_{Rm} on the values of $\tilde{\sigma}_H$ and $\tilde{\sigma}_O$ is shown by a three-dimensional graph in Fig. 7. It is seen from Fig. 7 that γ_{Rm} is not the monotonic function of $\tilde{\sigma}_H$ and $\tilde{\sigma}_O$ and the variations of γ_{Rm} with $\tilde{\sigma}_H$ and $\tilde{\sigma}_O$ are approximately saddle-shaped. Besides, it can be clearly seen by comparing Fig. 7 (a) and 7 (b) that the value of γ_{Rm} not only depends on the values of $\tilde{\sigma}_H$ and $\tilde{\sigma}_O$, but also the temperatures of external heat reservoirs, which is consistent with the result obtained by Ref. [33].

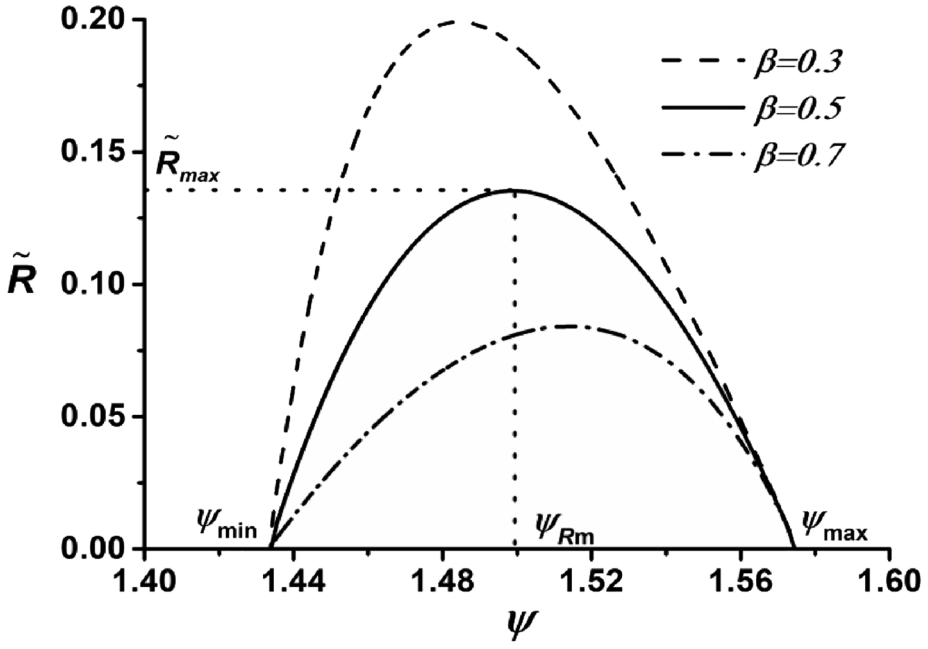

Fig. 4. The relation between optimized ψ and the corresponding $\tilde{R}$ for different values of β. Fixed parameters are $\tilde{\sigma}_H=\tilde{\sigma}_O=0.3$, $\alpha=0.5$, $\tilde{T}_H=3$ and $\tilde{T}_P=1.5$.

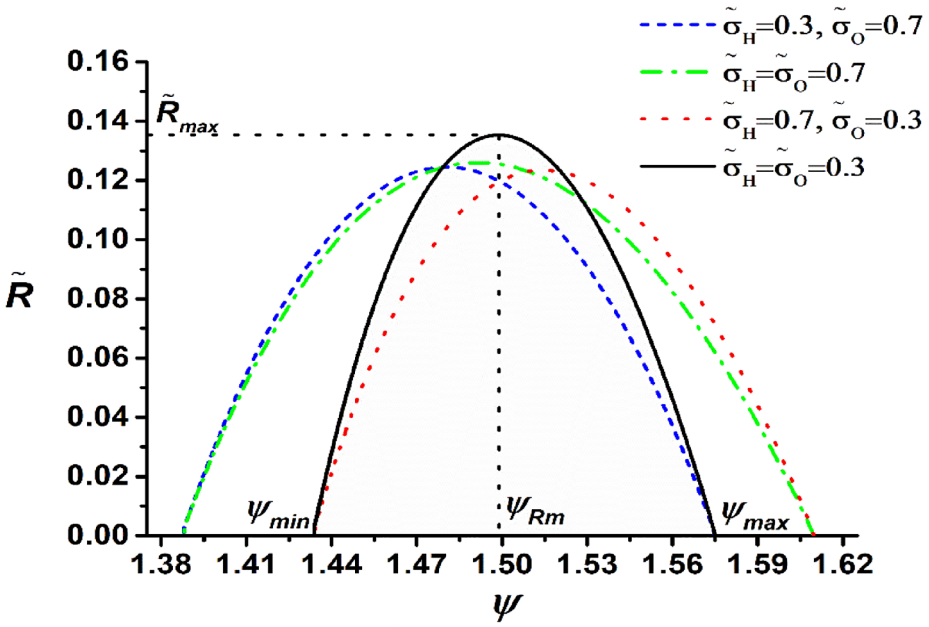

Fig. 5. The relation between optimized ψ and the corresponding $\tilde{R}$ for different values of $\tilde{\sigma}_H$ and $\tilde{\sigma}_O$. Fixed parameters are $\alpha = \beta = 0.5$, $\tilde{T}_H = 3$ and $\tilde{T}_P = 1.5$.

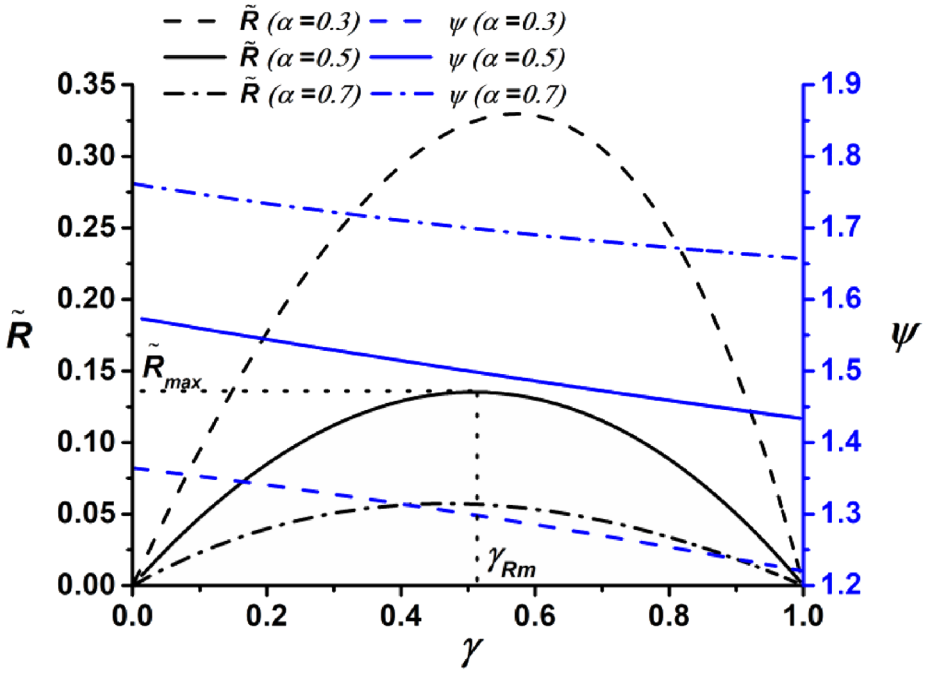

Fig. 6. The variations of the optimized ψ and the corresponding $\tilde{R}$ with γ for different values of α. Fixed parameters are $\tilde{\sigma}_H = \tilde{\sigma}_O = 0.3$, $\beta = 0.5$, $\tilde{T}_H = 3$ and $\tilde{T}_P = 1.5$.

3.3. The behaviors of ψ_{Rm} and $\tilde{R}_{\max}$

According to the analyses above, ψ_{Rm} and $\tilde{R}_{\max}$ are two important parameters accounting for the optimal operation of the system. Using Eqs. (6), (8), (9), (11), (13), the data in Fig. 3, and numerical calculation, one can plot the $\tilde{R}_{\max} - \psi_{Rm}$ curves for different $\tilde{\sigma}_H$ and $\tilde{\sigma}_O$ and the variations of $\tilde{R}_{\max}$ and ψ_{Rm} with α and C for given values of other parameters, as shown in Fig. 8(a) and (b).

It can be found out from Fig. 8(a) that $\tilde{R}_{\max}$ decreases as ψ_{Rm} increases in both symmetry and asymmetry dissipation situations. Consequently, a compromise between heat load and COP should be made in the design of a practical three-heat-source heat pump. Specifically, the ratio of the heat exchange area of condenser (evaporator) to that of generator (absorber) for the absorption heat pump, the ratio of the heat exchange area of condenser (evaporator) to that of adsorber (desorber) for the adsorption heat pump, and the ratio of the heat exchange area of evaporator to that of generator for the ejector heat pump should be chosen based on the data in Fig. 8(b) to satisfy the performance requirement.

It is worth to point out that the above relations between ψ_{Rm}, $\tilde{R}_{\max}$, and $C(\alpha)$ are well different from the thermally driven refrigerators [46] in which the maximum cooling power is not a monotonic function of size ratio and the corresponding COP. Namely, there exists an optimal design which makes the cooling power of thermally driven refrigerator attain its globally maximum value and the corresponding COP can be determined. This distinctive feature does not appear in the thermally driven heat pump devices. Accordingly, different strategies in the design of practical devices should be selected. In particular, all values of

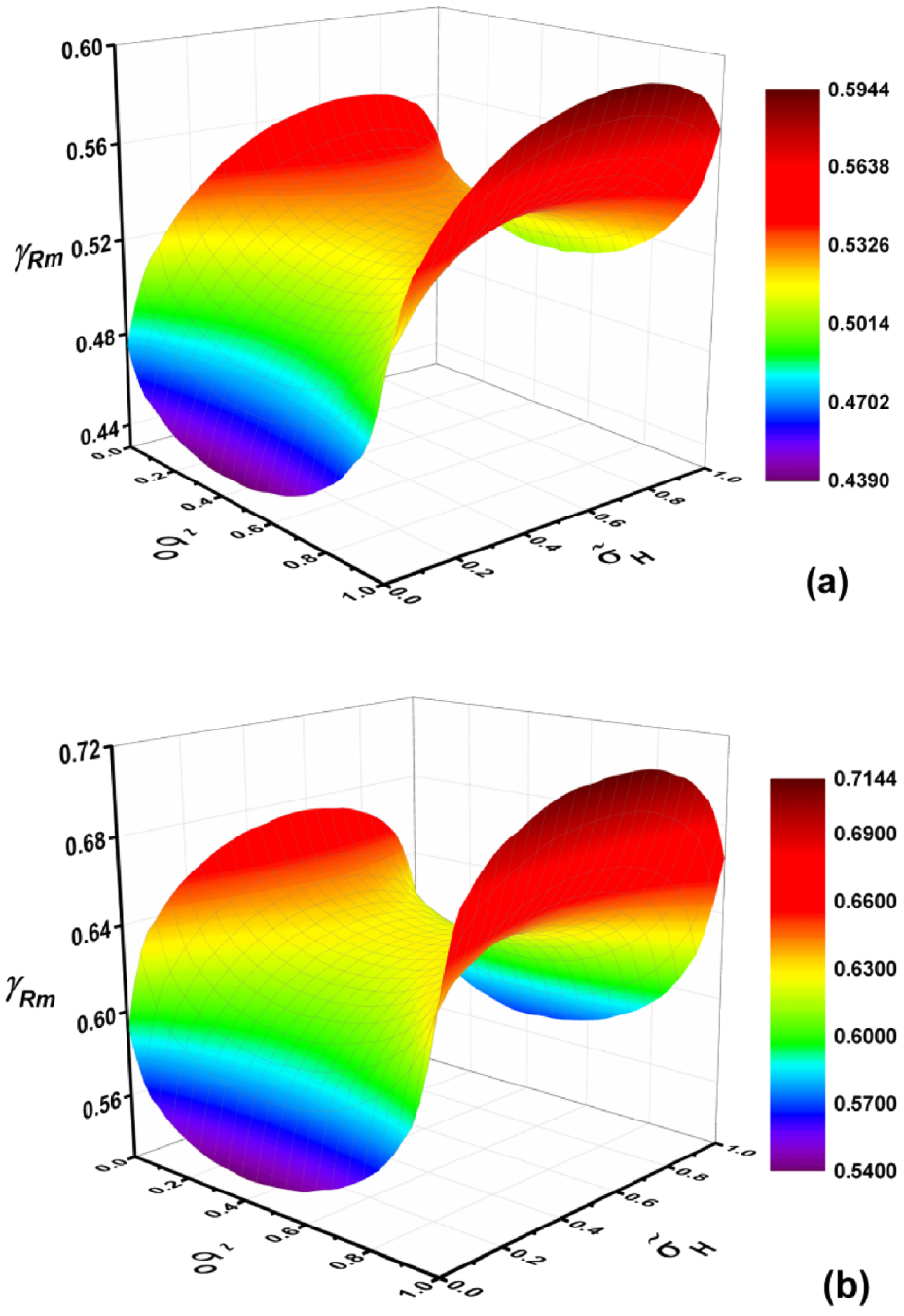

Fig. 7. Three-dimensional variations of γ_{Rm} with $\tilde{\sigma}_H$ and $\tilde{\sigma}_O$, $\alpha = \beta = 0.5$, $\tilde{T}_P = 1.5$, (a) $\tilde{T}_H = 3$, and (b) $\tilde{T}_H = 2$.

the size ratio between 0 and C_r are physically acceptable for thermally heat pump, while for thermally driven refrigerator the size ratio should be controlled in the region between the optimal size ratio and the size ratio under reversible limit [46].

Based on the data in Fig. 5, the three-dimensional variations of ψ_{Rm} and $\tilde{R}_{\max}$ with $\tilde{\sigma}_H$ and $\tilde{\sigma}_O$ are generated with the help of numerical calculation, which are shown in Fig. 9(a) and (b), respectively. It can be realized from Fig. 9(a) that ψ_{Rm} increases monotonically as $\tilde{\sigma}_H$ grows for a given $\tilde{\sigma}_O$ but it decreases monotonically as $\tilde{\sigma}_O$ increases for a given value of $\tilde{\sigma}_H$. This result agrees with it could be expected because when $\tilde{\sigma}_H \to 1$ and $\tilde{\sigma}_O \to 0$ more heat can be released into heated space while less heat is absorbed from the heat reservoir with high temperature for given other parameters, which can be known from Eqs. (2) to (5). Fig. 9 (b) shows that $\tilde{R}_{\max}$ is not a monotonic function of $\tilde{\sigma}_H$ and $\tilde{\sigma}_O$ and there exist optimal values of $\tilde{\sigma}_H$ and $\tilde{\sigma}_O$ at which $\tilde{R}_{\max}$ attains its minimum.

Using Eqs. (6), (8), (9), (11), (13), the data in Fig. 5, and numerical calculation, one can generate the curves of ψ_{Rm} varying with $\tilde{T}_H$ and $\tilde{T}_P$ for different values of α. More importantly, according to Figs. 4 and 9 (a), the upper bounds of the $\psi_{Rm} - \tilde{T}_H$ and $\psi_{Rm} - \tilde{T}_P$ curves for different values of α can be obtained by setting $\beta \to 1$, $\tilde{\sigma}_H \to 1$, and $\tilde{\sigma}_O \to 0$. Meanwhile, the lower bounds of the $\psi_{Rm} - \tilde{T}_H$ and $\psi_{Rm} - \tilde{T}_P$ curves for different values of α can be obtained by setting $\beta \to 0$, $\tilde{\sigma}_H \to 0$, and $\tilde{\sigma}_O \to 1$, which are shown in Fig. 10(a) and (b), where the $\psi_r - \tilde{T}_H$ and $\psi_r - \tilde{T}_P$ curves and the $\psi_{Rm} - \tilde{T}_H$ and $\psi_{Rm} - \tilde{T}_P$ curves at the condition of symmetry dissipation, namely, $\beta = 0.5$, $\tilde{\sigma}_H = 0.5$ and $\tilde{\sigma}_O = 0.5$, are also displayed. It is seen from Fig. 10 that both ψ_{Rm} and ψ_r increase with the increase of $\tilde{T}_H$ for a given value of $\tilde{T}_P$ and decrease with the increase of $\tilde{T}_P$ for a given value of $\tilde{T}_H$. Those behaviors are the expected results due to the fact that the difficulty to pump heat into the heated space increases with the increase of $\tilde{T}_P$ but decreases with the increase of $\tilde{T}_H$. As

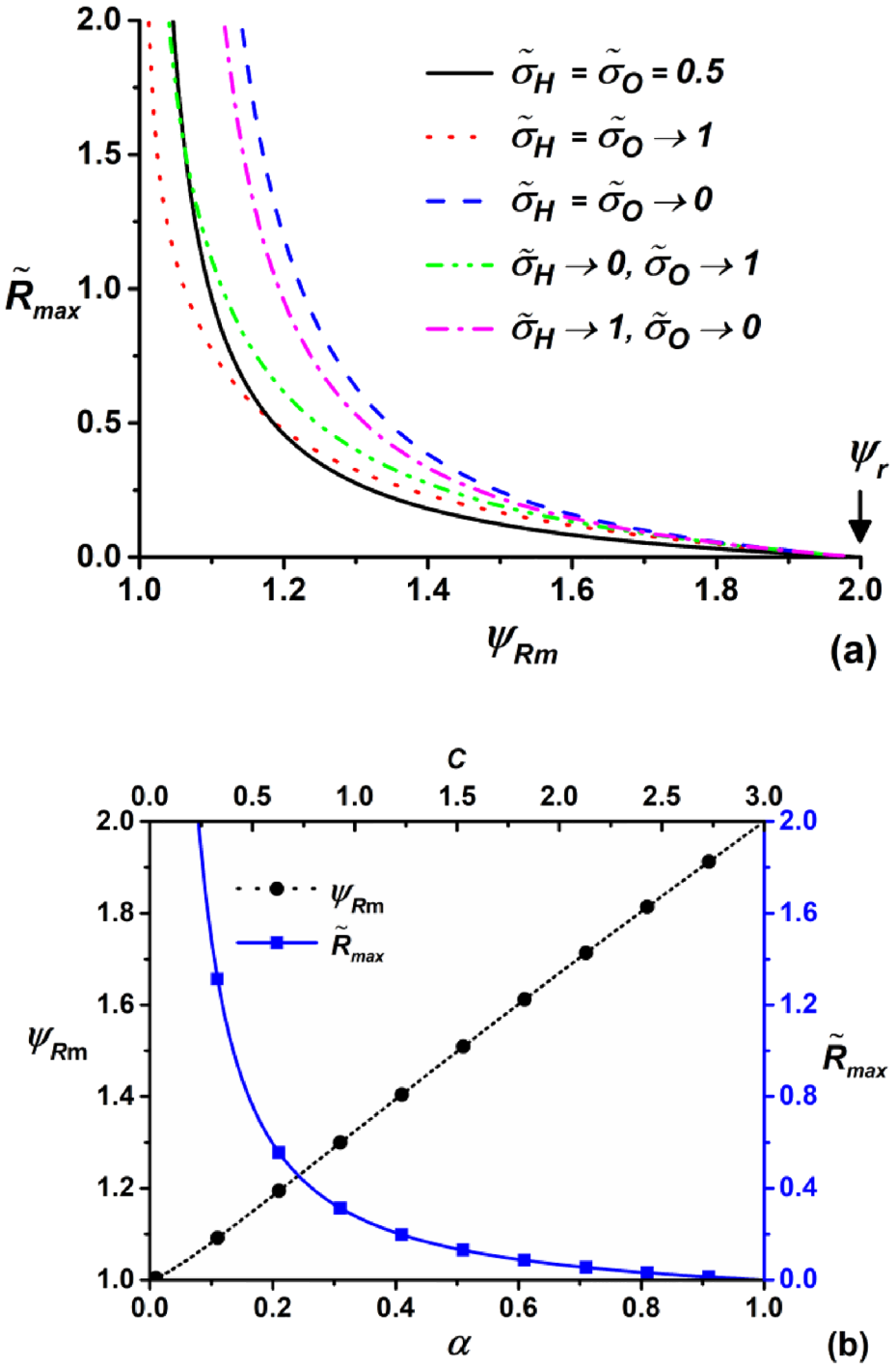

Fig. 8. (a) The variations of $\tilde{R}_{\max}$ with ψ_{Rm} for different values of $\tilde{\sigma}_H$ and $\tilde{\sigma}_O$, where $\alpha = \beta = 0.5$, $\tilde{T}_H = 3$ and $\tilde{T}_P = 1.5$. (b) The variations of $\tilde{R}_{\max}$ and ψ_{Rm} with α and C, where $\tilde{\sigma}_H = 0.3$, $\tilde{\sigma}_O = 0.3$, $\beta = 0.5$, $\tilde{T}_H = 3$ and $\tilde{T}_P = 1.5$.

a result, when $\tilde{T}_H = \tilde{T}_P$, $\psi_{Rm} = \psi_r = 1$, namely, the low-dissipation three-heat-source heat pump is disabled. Besides, for given values of $\tilde{T}_H$ and $\tilde{T}_P$, ψ_{Rm} increases with the increase of α.

It is noteworthy to point out that in Fig. 10, the values of $\tilde{T}_H$ and $\tilde{T}_P$ are not fixed. Therefore, the value of C should be changed according to the variations of $\tilde{T}_H$ or $\tilde{T}_P$ to keep the value of α constant. As a result, in order to exhibit the behaviors of ψ_{Rm} varying with $\tilde{T}_H$ and $\tilde{T}_P$ for one practical three-heat-source heat pump with constant ratio of the heat exchange areas of different components, the curves of $\psi_{Rm} - \tilde{T}_H$ and $\psi_{Rm} - \tilde{T}_P$ for given values of C are plotted by using Eqs. (6), (8), (9), (11), (13), the data in Fig. 5, and numerical calculation, which are shown in Fig. 11 (a) and (b).

In Fig. 11 (a) and (b), the $\psi_{Rm} - \tilde{T}_H$ and $\psi_{Rm} - \tilde{T}_P$ curves with same value of C from the top to the bottom correspond to the upper bound, symmetry dissipation, and lower bound, respectively. It can be found out from Fig. 11 (a) and (b) that the value ranges of $\tilde{T}_P$ and $\tilde{T}_H$ are limited by the condition $C \leqslant C_r$. Besides, the characteristics of the $\psi_{Rm} - \tilde{T}_H$ and $\psi_{Rm} - \tilde{T}_P$ curves for given values of C are more complicated than those in Fig. 10 (a) and (b). On the one hand, with the increase of $\tilde{T}_H$ and the decrease of $\tilde{T}_P$, the difficulty to pump heat into the heated space decreases, which can be realized from $(\partial\psi_r/\partial\tilde{T}_H)_{\tilde{T}_P} = \tilde{T}_P/[\tilde{T}_H^2(\tilde{T}_P - 1)] > 0$ and $(\partial\psi_r/\partial\tilde{T}_P)_{\tilde{T}_H} = -(\tilde{T}_H - 1)/[\tilde{T}_H(\tilde{T}_P - 1)^2] < 0$, respectively. On the other hand, for given

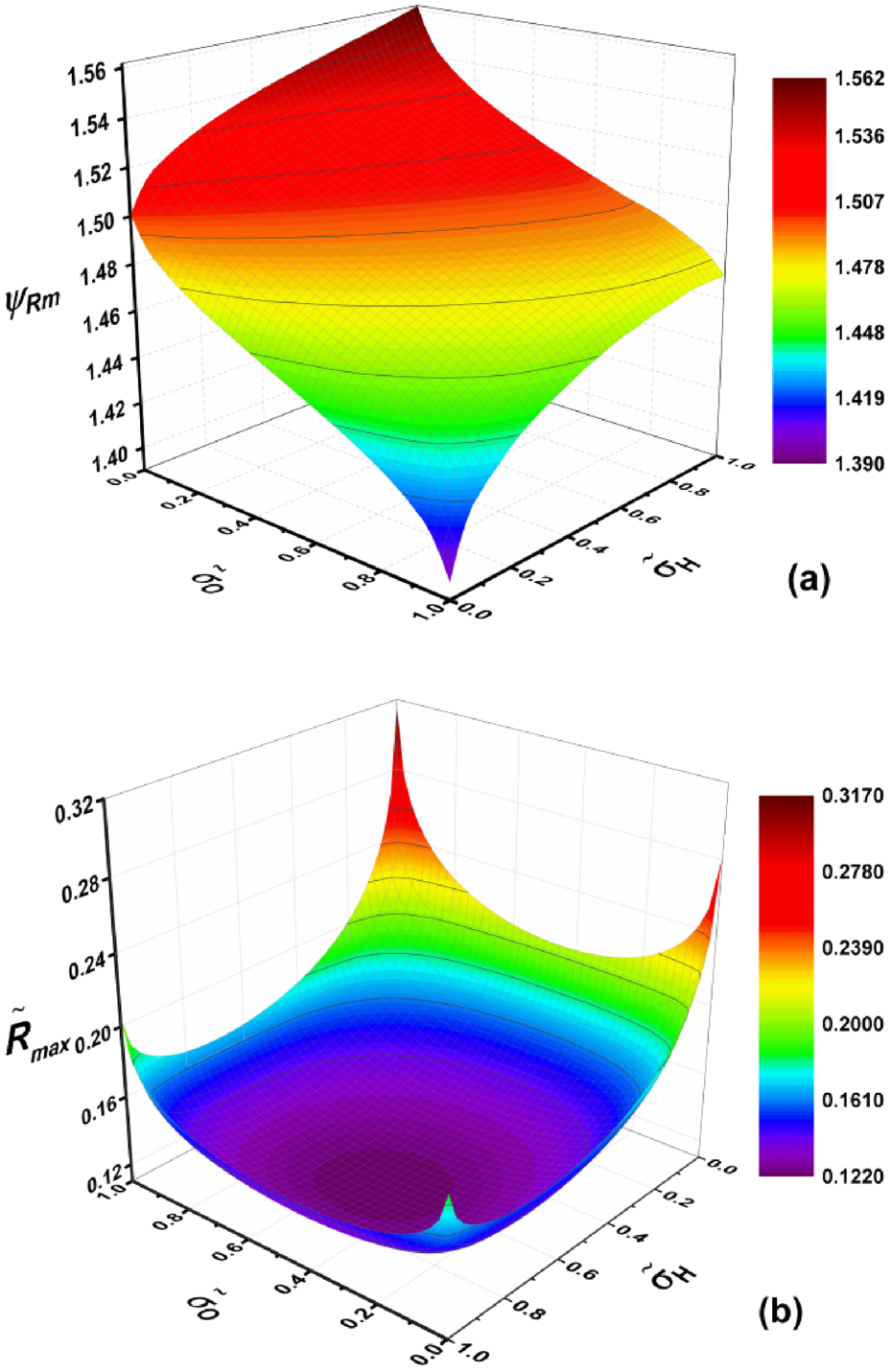

Fig. 9. Three-dimensional variations of (a) ψ_{Rm} and (b) $\tilde{R}_{\max}$ with $\tilde{\sigma}_H$ and $\tilde{\sigma}_O$, $\alpha = \beta = 0.5$, $\tilde{T}_H = 3$ and $\tilde{T}_P = 1.5$.

values of $\tilde{T}_P$ and $\tilde{T}_H$, with the increase of $\tilde{T}_H$ and the decrease of $\tilde{T}_P$, the irreversibility level of the global system increases, which can be realized from $(\partial\alpha/\partial\tilde{T}_H)_{C,\tilde{T}_P} = -C(\tilde{T}_P - 1)/(\tilde{T}_H - \tilde{T}_P)^2 < 0$ and $(\partial\alpha/\partial\tilde{T}_P)_{C,\tilde{T}_H} = C(\tilde{T}_H - 1)/(\tilde{T}_H - \tilde{T}_P)^2 > 0$. Besides, the effect of irreversibility increases from the upper bound to the lower bound gradually. Consequently, the behaviors of ψ_{Rm} with $\tilde{T}_H$ and ψ_{Rm} with $\tilde{T}_P$ depend on the trade-off between those factors mentioned above.

Fig. 11 (a) indicates that ψ_{Rm} is a monotonically decreasing function of $\tilde{T}_H$ for all three different situations. With the increase of $\tilde{T}_H$, the absolute values of the slope of the curves decrease. Nevertheless, the behaviors of ψ_{Rm} with $\tilde{T}_P$ for three different cases show different trends, which can be seen from Fig. 11 (b). Specifically, the upper bound of $\psi_{Rm} - \tilde{T}_P$ curves decrease with the increase of $\tilde{T}_P$ due to the less influence from irreversibility than two other curves. On the contrary, the lower bound of $\psi_{Rm} - \tilde{T}_P$ curves and the $\psi_{Rm} - \tilde{T}_P$ curves under symmetry dissipation show positive slopes. For given values of $\tilde{T}_H$ and $\tilde{T}_P$, the value of ψ_{Rm} increases with the increase of C.

It is noteworthy that the bounds of the COP at maximum heat load presented in Figs. 10 and 11 are obtained under different conditions and have different physical meanings comparing to the COP bounds at maximum cooling power for thermally driven refrigerators obtained in Ref. [46] due to the lack of optimal value of size ratio, even though some of the curves look alike. Specifically, in Ref. [46], every point in the COP bounds at maximum cooling power were generated for optimal

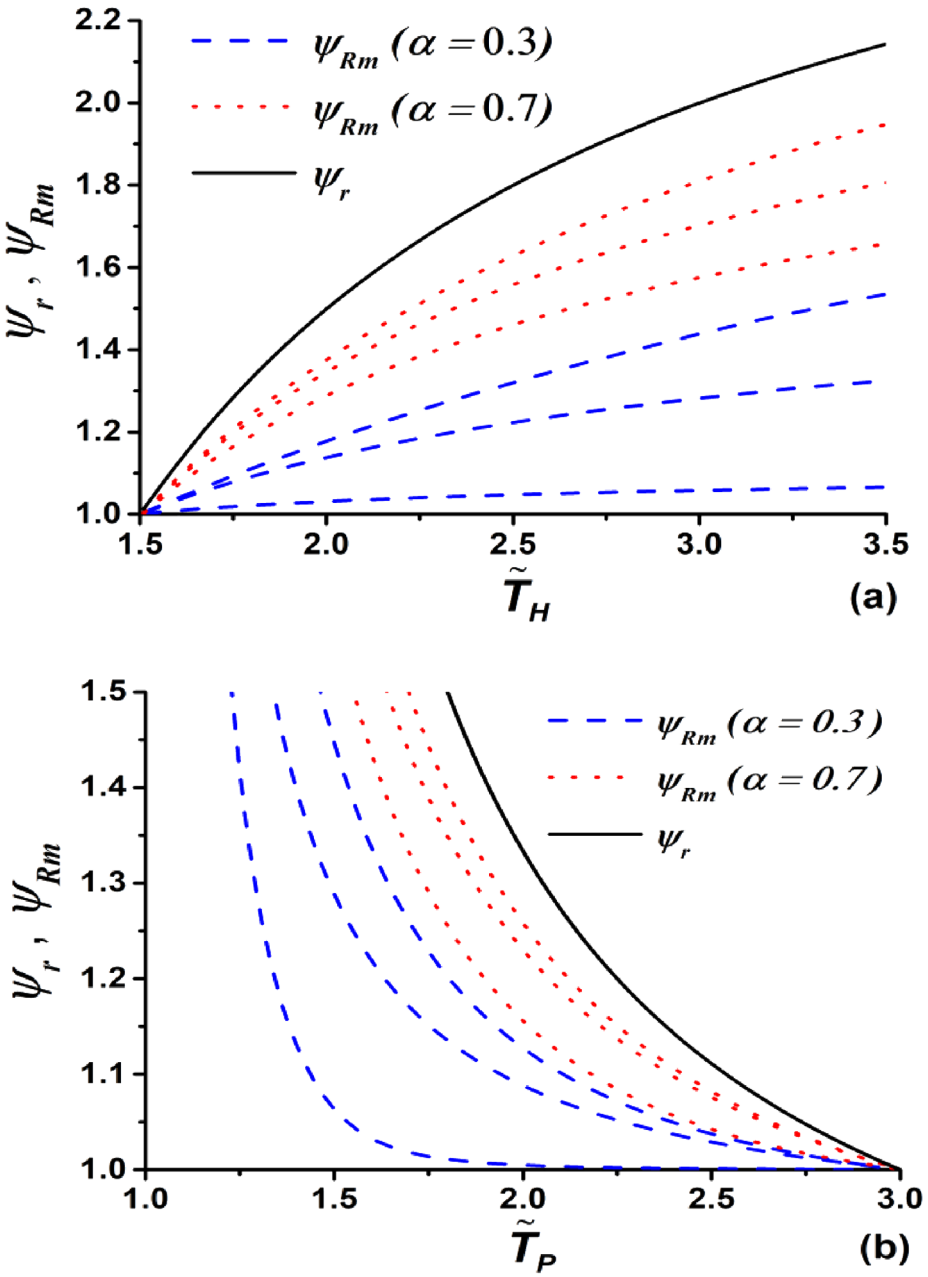

Fig. 10. The curves of ψ_{Rm} and ψ_r varying with (a) $\tilde{T}_H$ and (b) $\tilde{T}_P$ for different α, with $\beta \to 1$, $\tilde{\sigma}_H \to 1$, and $\tilde{\sigma}_O \to 0$ for the upper bound; $\beta \to 0$, $\tilde{\sigma}_H \to 0$, and $\tilde{\sigma}_O \to 1$ for the lower bound; and $\beta = 0.5$, $\tilde{\sigma}_H = 0.5$, and $\tilde{\sigma}_O = 0.5$ for the curve between upper and lower bounds (a) $\tilde{T}_P = 1.5$, and (b) $\tilde{T}_H = 3$.

size ratios (depending on the operating temperatures). However, in Figs. 10 and 11, the upper and lower bounds are plotted for given values of size ratio and α.

3.4. Discussions

In this subsection, two additional points which reinforce the validity and generality of the low-dissipation model established above are explicitly analyzed. In addition, the limitations of the proposed model are discussed.

3.4.1. Extension for low-dissipation three-source chemical pump

With the help of low-dissipation assumptions, the performance characteristics of a three-source chemical pump consisting of a chemical pump driven by a chemical engine [48], which may be an analogue to the chemical processes inside a photosynthesis engine [49], can be also investigated.

For a low-dissipation three-source chemical pump consisting of a low-dissipation chemical engine working between two reservoirs with chemical potentials μ_H and μ_P ($\mu_H > \mu_P$) and a low-dissipation chemical pump working between two reservoirs with chemical potentials μ_P and μ_O ($\mu_P > \mu_O$), the energy absorbed from reservoir with high chemical potential by the chemical engine, the energies released into reservoir with intermediate chemical potential by the chemical engine and the chemical pump, and the energy absorbed from reservoir with low chemical potential by the chemical pump per cycle can be expressed as [36]

$$U_H = U_{Hr}\left(1 - \frac{\sigma_H}{t_H}\right) = \mu_H \Delta N_{ce}\left(1 - \frac{\sigma_H}{t_H}\right) \tag{15}$$

$$U_{PH} = U_{PHr}\left(1 + \frac{\sigma_{PH}}{t_{PH}}\right) = \mu_P \Delta N_{ce}\left(1 + \frac{\sigma_{PH}}{t_{PH}}\right) \tag{16}$$

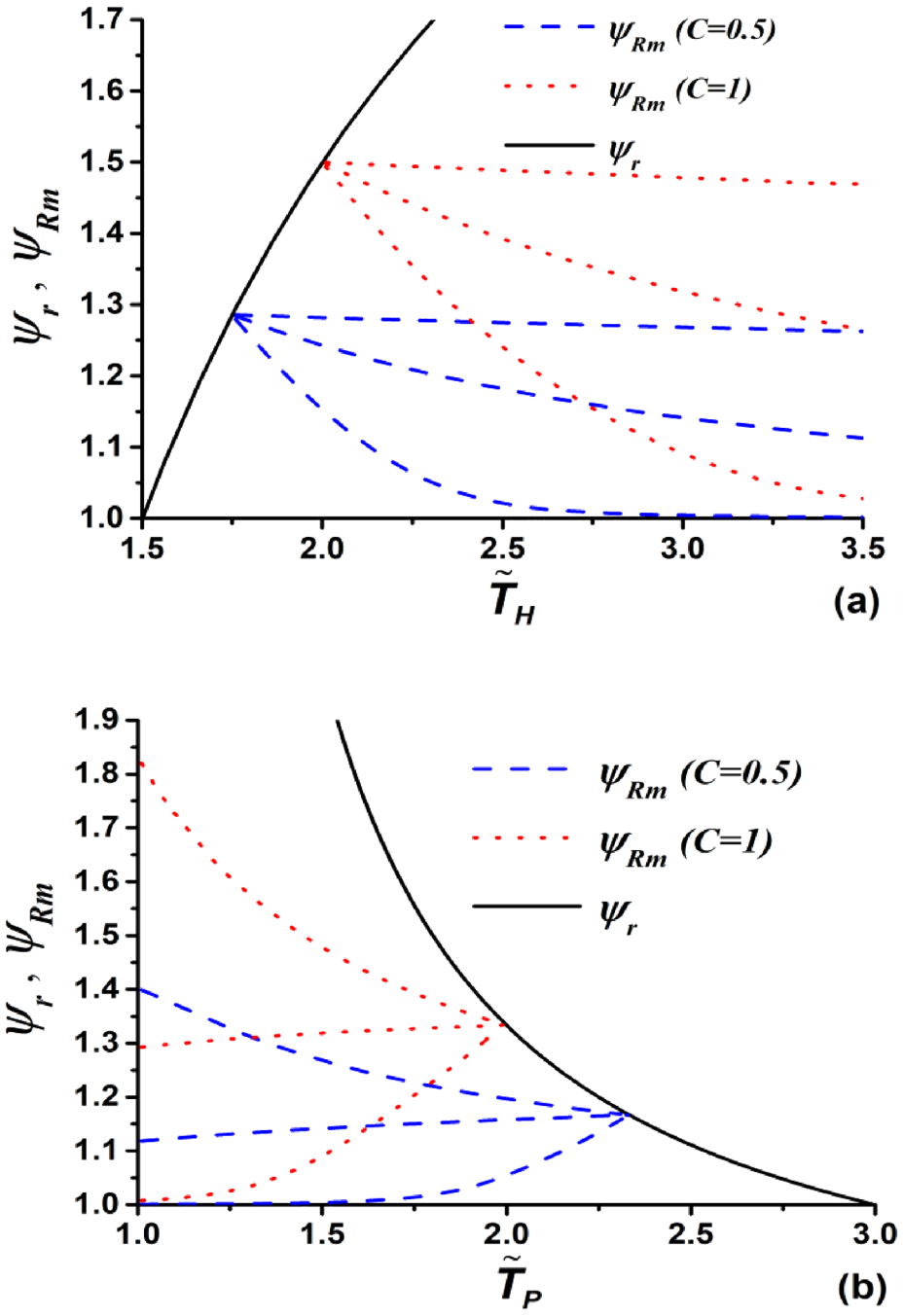

Fig. 11. The variations of ψ_{Rm} and ψ_r with (a) $\tilde{T}_H$ and (b) $\tilde{T}_P$ for different C, with $\beta \to 1$, $\tilde{\sigma}_H \to 1$, and $\tilde{\sigma}_O \to 0$ for the upper bound; $\beta \to 0$, $\tilde{\sigma}_H \to 0$, and $\tilde{\sigma}_O \to 1$ for the lower bound; and $\beta = 0.5$, $\tilde{\sigma}_H = 0.5$, and $\tilde{\sigma}_O = 0.5$ for the curve between upper and lower bounds (a) $\tilde{T}_P = 1.5$, and (b) $\tilde{T}_H = 3$.

$$U_{PO} = U_{POr}(1 + \frac{\sigma_{PO}}{t_{PO}}) = \mu_P \Delta N_{cp}(1 + \frac{\sigma_{PO}}{t_{PO}}) \tag{17}$$

and

$$U_O = U_{Or}(1 - \frac{\sigma_O}{t_O}) = \mu_O \Delta N_{cp}(1 - \frac{\sigma_O}{t_O}) \tag{18}$$

respectively, where $U_{Hr} = \mu_H \Delta N_{ce}$, $U_{PHr} = \mu_P \Delta N_{ce}$, $U_{POr} = \mu_P \Delta N_{cp}$, and $U_{Or} = \mu_O \Delta N_{cp}$ are, respectively, the corresponding exchanged energies under reversible condition, ΔN_{ce} and ΔN_{cp} are, respectively, the corresponding masses transmitted by the chemical engine and the chemical pump under reversible condition and may represent the size of the chemical engine and the chemical pump. Besides, t_H, t_{PH}, t_{PO}, and t_O denote, respectively, the time durations of four mass transfer processes pre cycle, σ_H, σ_{PH}, σ_{PO}, and σ_O are four corresponding coefficients including the irreversibility information.

By comparing Eqs. (2)–(5) with Eqs. (15)–(18), it can be found out that the performance characteristics of the low-dissipation three-heat-source heat pump obtained in Sections 2 and 3 can be directly used to discuss the low-dissipation three-source chemical pump if only $Q_{Hr} = T_H \Delta S_{he}$, $Q_{PHr} = T_P \Delta S_{he}$, $Q_{POr} = T_P \Delta S_{hp}$, and $Q_{Or} = T_O \Delta S_{hp}$ are replaced by $U_{Hr} = \mu_H \Delta N_{ce}$, $U_{PHr} = \mu_P \Delta N_{ce}$, $U_{POr} = \mu_P \Delta N_{cp}$, and $U_{Or} = \mu_O \Delta N_{cp}$, respectively.

3.4.2. The limit of $T_H \to \infty$: Conventional compression heat pump.

According to Ref. [50], when $T_H \to \infty$ the high-temperature heat reservoir become a work source. As a result, the low-dissipation three-heat-source heat pump shown in Fig. 2 goes back to a traditional compression low-dissipation heat pump driven by work working

between the heated space (T_P) and environment (T_O). In this case, $Q_H = W$, $Q_{PH} = 0$, $t_H = 0$, $\sigma_H = 0$, $t_{PH} = 0$, $\sigma_{PH} = 0$. Consequently, one has $C = C_r \to \infty$, which means that the heat engine is not adopted. In addition, Eqs. (1), (8), and (9) can be rewritten as

$$\psi_r = \frac{T_P}{T_P - T_O} \tag{19}$$

$$R = \frac{T_P \Delta S_{hp}(1 + \frac{\sigma_{PO}}{t_{PO}})}{t_{PO} + t_O} \tag{20}$$

and

$$\psi = \frac{T_P(1 + \frac{\sigma_{PO}}{t_{PO}})}{T_P(1 + \frac{\sigma_{PO}}{t_{PO}}) - T_O(1 - \frac{\sigma_O}{t_O})} \tag{21}$$

which are the COP of reversible compression heat pump, heat load, and COP of the low-dissipation compression heat pump [51], respectively.

3.4.3. The limitations of the proposed model

The proposed model has the advantages of generality and wide applicability, but its limitations are obvious as well. Firstly, instead of specifying the heat-transfer laws, the associated dissipation coefficients in each heat-transfer processes are introduced. Nevertheless, as mentioned in Section 2.1, the physical meanings of the dissipation coefficients are somewhat abstract and hard to be determined for realistic thermal devices. The relations between dissipation coefficients and Onsager coefficients have been explored for heat engine [52] and refrigerator [43], respectively. However, the practical meanings of the dissipation coefficients are still ambiguous and further investigations are necessary. Secondly, according to the practical meanings of reversible entropies, for an absorption heat pump the heat exchange areas of condenser and evaporator (ΔS_{hp}) are required to be the same as well as the heat exchange areas of generator and absorber (ΔS_{he}). This requirement usually cannot be satisfied for the practical absorption heat pump in which the heat exchange areas of each components are different [8]. For adsorption and ejector heat pumps, there are similar deviations between the proposed model and the practical devices. Thirdly, in the discussions of the optimal performances of thermally driven heat pumps, dimensionless time durations and heat load are introduced since the values of dissipation coefficients are hard to be determined for realistic devices. Consequently, some of the obtained results have theoretical significances but their practical implementation need further studies.

4. Concluding remarks

In this paper, a more universal thermodynamic model without considering the specific law of heat-transfer has been established based on low-dissipation assumption to investigate the performance characteristics, design, and operation strategies of thermally driven heat pumps, mainly including absorption, adsorption, and ejector heat pumps. Four important findings are listed below:

1. The joint description of the low-dissipation three-heat-source heat pump in terms of both dissipation and temporal symmetries/asymmetries was proposed, which extends the theoretical application of low-dissipation thermodynamic model.
2. The optimal performance characteristics and the optimal operations of the thermally driven heat pumps were discussed and determined by introducing an important parameter $C = \Delta S_{hp}/\Delta S_{he}$ denoting the size ratio of the heat pump to the heat engine. This parameter stressed the practical meanings of reversible entropy changes inside the low-dissipation model and connected the two subsystems inside the overall system (Eq. (6)). Moreover, the different performances, operation strategies, and design constraints between low-dissipation heat pump and refrigerator have been underlined.
3. Based on the deatiled discussions about the performance of the thermally driven heat pumps, the bounds of the COP at maximum heat load were obtained at two extreme asymmetry conditions.
4. A further extension and a limit case of the proposed model have been presented from which the similarity between the low-dissipation three-source chemical pump and the low-dissipation three-heat-source heat pump was realized and the validity and generality of the proposed model were highlighted. Besides, the limitations of the proposed model are indicated.

It is reasonable to believe the proposed model and the significant results obtained further develop the low-dissipation model and provide a novel and useful description for the operation and design of practical thermally driven heat pumps.

Declaration of Competing Interest

The authors declare that they have no known competing financial interests or personal relationships that could have appeared to influence the work reported in this paper.

Acknowledgements

This work has been supported by the National Natural Science Foundation of China (No. 11405032) and Junta de Castilla y León of Spain under project SA017P17. J.G.A. acknowledges University of Salamanca contract 2017/X005/1.

References

[1] Chu S, Majumdar A. Opportunities and challenges for a sustainable energy future. Nature 2012;488:294–303.
[2] Rahbar K, Mahmoud S, Al-Dadah RK, Moazami N, Mirhadizadeh SA. Review of organic Rankine cycle for small-scale applications. Energy Convers Manage 2017;134:135–55.
[3] Zhang H, Kong W, Dong F, Xu H, Chen B, Ni M. Application of cascading thermoelectric generator and cooler for waste heat recovery from solid oxide fuel cells. Energy Convers Manage 2017;148:1382–90.
[4] Lee SW, Yang Y, Lee HW, Ghasemi H, Kraemer D, Chen G, et al. An electrochemical system for efficiently harvesting low-grade heat energy. Nat Commun 2014;5:3942.
[5] Xu ZY, Mao HC, Liu DS, Wang RZ. Waste heat recovery of power plant with large scale serial absorption heat pumps. Energy 2018;165:1097–105.
[6] Pan QW, Wang RZ. Study on boundary conditions of adsorption heat pump systems using different working pairs for heating application. Energy Convers Manage 2017;154:322–35.
[7] Zhang C, Lin J, Tan Y. A theoretical study on a novel combined organic Rankine cycle and ejector heat pump. Energy 2019;176:81–90.
[8] Wang M, Ferreira CAI. Absorption heat pump cycles with NH3-ionic liquid working pairs. Appl Energy 2017;204:819–30.
[9] Chen Z, Jin X, Shimizu A, Hihara E, Dang C. Effects of the nozzle configuration on solar-powered variable geometry ejectors. Sol Energy 2017;150:275–86.
[10] Baek S, Ko S, Song S, Ryu S. Numerical study of high-speed two-phase ejector performance with R134a refrigerant. Int J Heat Mass Tran 2018;126:1071–82.
[11] Wu W, Shi WX, Wang BL, Li XT. A new heating system based on coupled air source absorption heat pump for cold regions: energy saving analysis. Energy Convers Manage 2013;76:811–7.
[12] Xu C, Bai P, Xin T, Hu Y, Xu G, Yang Y. A novel solar energy integrated low-rank coal fired power generation using coal pre-drying and an absorption heat pump. Appl Energy 2017;200:170–9.
[13] Padilla D, Rodríguez L. Application of absorption heat pumps to multi-effect distillation: a case study of solar desalination. Desalination 2007;212:294–302.
[14] Jing R, Wang M, Wang W, Brandon N, Li N, Chen J, et al. Economic and environmental multi-optimal design and dispatch of solid oxide fuel cell based CCHP system. Energy Convers Manage 2017;154:365–79.
[15] Hultén M, Berntsson T. The compression/absorption heat pump cycle-conceptual design improvements and comparisons with the compression cycle. Int J Refrig 2002;25:487–97.
[16] Yan G, Bai T, Yu J. Energy and exergy efficiency analysis of solar driven ejector-compressor heat pump cycle. Sol Energy 2016;125:243–55.
[17] Nguyen HQ, Shabani B. Proton exchange membrane fuel cells heat recovery opportunities for combined heating/cooling and power applications. Energy Convers Manage 2020;204:112328.
[18] Zare V, Takleh HR. Novel geothermal driven CCHP systems integrating ejector transcritical CO_2 and Rankine cycles: thermodynamic modeling and parametric study. Energy Convers Manage 2020;205:112396.
[19] Dai E, Jia T, Dai Y. Theoretical and experimental investigation on a GAX-Based

NH3-H2O absorption heat pump driven by parabolic trough solar collector. Sol Energy 2020;197:498–510.
[20] Huang FF. Engineering thermodynamics. New York: Macmillan; 1976.
[21] Chen J, Yan Z. Equivalent combined systems of three-heat-source heat pumps. J Chem Phys 1989;90:4951–5.
[22] Göktun S. The effect of irreversibilities on the performance of a three-heat-source heat pump. J Phys D: Appl Phys 1996;29:2823–5.
[23] Chen J. Optimal performance analysis of irreversible cycles used as heat pumps and refrigerators. J Phys D: Appl Phys 1997;30:582–7.
[24] Chen L, Wu C, Sun F. Optimal coefficient of performance and heating load relationship of a three-heat-reservoir endoreversible heat pump. Energy Convers Manage 1997;38:727–33.
[25] Zhao X, Fu L, Zhang S. General thermodynamic performance of irreversible absorption heat pump. Energy Convers Manage 2011;52:494–9.
[26] Wu S, Lin G, Chen J. Optimum thermoeconomic and thermodynamic performance characteristics of an irreversible three-heat-source heat pump. Renew Energy 2005;30:2257–71.
[27] Ahmadi MH, Ahmadi MA, Mehrpooya M, Sameti M. Thermo-ecological analysis and optimization performance of an irreversible three-heat-source absorption heat pump. Energy Convers Manage 2015;90:175–83.
[28] Chen X, Wang Y, Zhou Y. Equivalent power output and parametric optimum design of a PEM fuel cell-based hybrid system. Int J Electr Power Energy Syst 2014;63:429–33.
[29] Davis GW, Wu C. Optimal performance of a geothermal heat-engine-driven heat-pump system. Energy 1994;19:1219–23.
[30] Chen J. Optimal performance characteristics of a solar-driven heat pump at maximum COP. Energy Convers Manage 1994;35:1009–14.
[31] Curzon FL, Ahlborn B. Efficiency of a Carnot engine at maximum power output. Am J Phys 1975;43:22–4.
[32] Chen L, Yan Z. The effect of heat-transfer law on performance of a two-heat-source endoreversible cycle. J Chem Phys 1989;90:3740–3.
[33] Esposito M, Kawai R, Lindenberg K, Van den Broeck C. Efficiency at maximum power of low-dissipation Carnot engines. Phys Rev Lett 2010;105:150603.
[34] Gonzalez-Ayala J, Medina A, Roco JMM, Calvo-Hernández A. Entropy generation and unified optimization of Carnot-like and low-dissipation refrigerators. Phys Rev E 2018;97:022139.
[35] Singh V, Johal RS. Low-dissipation Carnot-like heat engines at maximum efficient power. Phys Rev E 2018;98:062132.
[36] Guo J, Wang Y, Chen J. General performance characteristics and parametric optimum bounds of irreversible chemical engines. J Appl Phys 2012;112:103504.
[37] Wang J, He J, Wu Z. Efficiency at maximum power output of quantum heat engines under finite-time operation. Phys Rev E 2012;85:031145.
[38] De Tomás C, Roco JMM, Calvo-Hernández A, Wang Y, Tu ZC. Low-dissipation heat devices: unified trade-off optimization and bounds. Phys Rev E 2013;87:012105.
[39] Gonzalez-Ayala J, Calvo-Hernández A, Roco JMM. From maximum power to a trade-off optimization of low-dissipation heat engines: Influence of control parameters and the role of entropy generation. Phys Rev E 2017;95:022131.
[40] Gonzalez-Ayala J, Calvo-Hernández A, Roco JMM. Irreversible and endoreversible behaviors of the LD-model for heat devices: the role of the time constraints and symmetries on the performance at maximum χ figure of merit. J Stat Mech 2016;2016:073202.
[41] Calvo-Hernández A, Medina A, Roco JMM. Time, entropy generation, and optimization in low-dissipation heat devices. New J Phys 2015;17:075011.
[42] Ma YH, Xu D, Dong H, Sun C. Universal constraint for efficiency and power of a low-dissipation heat engine. Phys Rev E 2018;98:042112.
[43] Izumida Y, Okuda K, Roco JMM, Calvo-Hernández A. Heat devices in nonlinear irreversible thermodynamics. Phys Rev E 2015;91:052140.
[44] Johal RS. Heat engines at optimal power: Low-dissipation versus endoreversible model. Phys Rev E 2017;96:012151.
[45] Schmiedl T, Seifert U. Efficiency at maximum power: an analytically solvable model for stochastic heat engines. Europhys Lett 2008;81:20003.
[46] Guo J, Yang H, Zhang H, Gonzalez-Ayala J, Roco JMM, Medina A, et al. Thermally driven refrigerators: Equivalent low-dissipation three-heat-source model and comparison with experimental and simulated results. Energy Convers Manage 2019;198:111917.
[47] Yang P, Zhang H. Parametric analysis of an irreversible proton exchange membrane fuel cell/absorption refrigerator hybrid system. Energy 2015;85:458–67.
[48] Lin G, Chen J, Hua B. Optimal analysis on the performance of a chemical engine-driven chemical pump. Appl Energy 2002;72:359–70.
[49] De Vos A. The endoreversible theory of solar energy conversion: a tutorial. Sol Energy Mater Sol Cells 1993;31:75–93.
[50] Andresen B, Salamon P, Berry RS. Thermodynamics in finite time: extremals for imperfect heat engines. J Chem Phys 1977;66:1571–7.
[51] Guo J, Cai L, Yang H, Lin B. Performance characteristics and parametric optimizations of a weak dissipative pumped thermal electricity storage system. Energy Convers Manage 2018;157:527–35.
[52] Izumida Y, Okuda K. Efficiency at maximum power of minimally nonlinear irreversible heat engines. Europhys Lett 2012;97:10004.